

Nature and significance of a Cambro-Ordovician high-K, calc-alkaline sub-volcanic suite: the late- to post-orogenic Motru Dyke Swarm (Southern Carpathians, Romania)

Olivier Féménias · Tudor Berza · Mihai Tatu ·
Hervé Diot · Daniel Demaiffe

Received: 16 January 2006 / Accepted: 10 January 2007 / Published online: 14 March 2007
© Springer-Verlag 2007

Abstract The Motru Dyke Swarm intrudes the Precambrian Danubian basement of the Southern Carpathians (Romania). It is a marker of a sub-volcanic event that occurred during the early Palaeozoic (Cambrian to Ordovician). The geographical distribution of dykes on a ~2,000 km² area is heterogeneous; several areas of high dyke density have been the subject of a detailed petrological and geochemical study. Taken altogether, the 150 samples define a single complete magmatic series, from basaltic andesite to rhyolite. Whole-rock major element variations show a medium- to high-K, calc-alkaline magmatic suite. The compositional variations and the general decrease of trace element contents (both compatible and incompatible, including REEs) from basaltic andesite to rhyolite are consistent with 1) the fractionation of the

observed phenocryst assemblages, Ca-amphibole (Tivargasite to magnesiohornblende) followed by intermediate plagioclase, clinopyroxene and accessory biotite and quartz and 2) the absence of lower and/or upper crustal contamination. Trace elements diagrams display typical arc patterns (LILE, Pb and LREE enrichment and relative depletion in Nb-Ta, Zr-Hf and Ti). The Th/U, Nb/Ta and Zr/Hf ratios are constant and close to the mantle values throughout the whole series, which argues that the parental magma was generated from a single and homogeneous enriched lithospheric mantle source. The field regional evidence implies that melting occurred during a late- to post-orogenic period of lithospheric extension, and thus took place quite lately after the cessation of Pan-African subduction.

Keywords Dyke Swarm · Calc-alkaline · Late- to post-orogenic · Geochemistry · Romania

O. Féménias (✉) · D. Demaiffe
Laboratoire de Géochimie Isotopique et Géodynamique
Chimique, DSTE, Université Libre de Bruxelles (U.L.B.)
(CP 160/02), 50, av. Roosevelt, 1050 Bruxelles, Belgium
e-mail: ofemenia@ulb.ac.be

T. Berza
Institutul Geologic al României, 1, Caransebeș str.,
București 78344, Romania

M. Tatu
“Sabba S. Ștefănescu” Institute of Geodynamics
of the Romanian Academy 19-21, Jean Louis Calderon str.,
București 37 70201, Romania

H. Diot
Université de La Rochelle, av. M. Crépeau,
17042 La Rochelle cedex 1, France

H. Diot
UMR CNRS 6112, UFR des Sciences et Techniques,
BP 92208, 44322 Nantes Cedex 3, France

Introduction

High-K calc-alkaline suites display a large compositional range, both in volcanic rocks (basalt, andesite, dacite to rhyolite and their sub-volcanic analogues, commonly occurring as dyke swarms) and in their plutonic equivalents (gabbro, diorite, granodiorite to granite). They are reported to occur in different tectonic settings, from subduction-related arcs to post-collisional zones, e.g. the magmatism of the actual continent–continent collision zone in Turkey (Akay and Erdogan 2004), Iran (Aftabi and Atapour 2000) and Tibet (Nomade et al. 2004). It is a common practice to use geochemical discrimination diagrams (e.g. Pearce et al. 1984) to infer the geotectonic setting during the emplacement of magmatic suites of rocks. In many studies, there

are no structural data to confirm the conclusion deduced from geochemistry. We will show in this paper that geochemical data cannot always be used directly and unambiguously as geotectonic marker.

In the North-Gondwanian terranes and in Europe, the Early Ordovician period is classically considered as a period of extension, illustrated by the expansion of the Rheic ocean and by the first breakaway of peri-Gondwana terranes (first stage of Palaeo-Tethys opening: Stampfli and Borel 2002; von Raumer et al. 2003). Nevertheless, the newly formed small continental blocks at the northern margin of Gondwana (i.e. Armorica, Avalonia and/or European Hunic terranes) and the northern margin of the Gondwana megablock itself (i.e. Egyptian Sinai) are characterized by a calc-alkaline magmatic activity (Abdel-Rahman 1995). The geodynamic interpretation of this magmatism (active margin and/or extension, rifting) is still debated (Mattauer 2004 for the French Ordovician granitoids).

Palaeozoic (Early Cambrian to late-Ordovician) dyke swarms have been described in Northern Egypt (Abdel-Rahman and Doig 1987; Abdel-Rahman 1995) and recognized in the Pre-Variscan (Pan-African) basement of the Lower Danubian Alpine unit in the Southern Carpathians of Romania (Berza and Seghedi 1975). The latter gave the first comprehensive field and petrographic description of what they called “The Pre-Silurian Motru Dyke Swarm” (MDS). These dykes crosscut the post-collisional Pan-African granitoid plutons (Liégeois et al. 1996) and are covered by anchimetamorphic (=very low metamorphic grade) Upper Ordovician-Silurian sediments. They were clearly intruded in a late- to post-orogenic tectonic setting. However, the regional distribution of the numerous dykes in the field, as well as detailed petrological and geochemical data, are lacking, so that the magmatic differentiation processes and the source of the parental magma have not been discussed yet. This is the topic of this paper. Our objective is also to use the Motru Dyke Swarm as a magmatic marker and its geochemical signature as a geodynamic tracer.

Geological setting

The Southern Carpathians Alpine nappe structure

The South Carpathian Alpine belt (Fig. 1) results from the stacking of two (Getic and Danubian) major units (composed of a crystalline basement locally covered by Palaeozoic and Mesozoic sediments) thrust upon the Moesian cratonic platform in the Upper Cretaceous to Tertiary times. These units were partly covered by Cainozoic sediments, marked by a major unconformity. The various Eoalpine (Cretaceous) Danubian nappes (Fig. 2) have been subdivided into the Upper and Lower Danubian (Berza

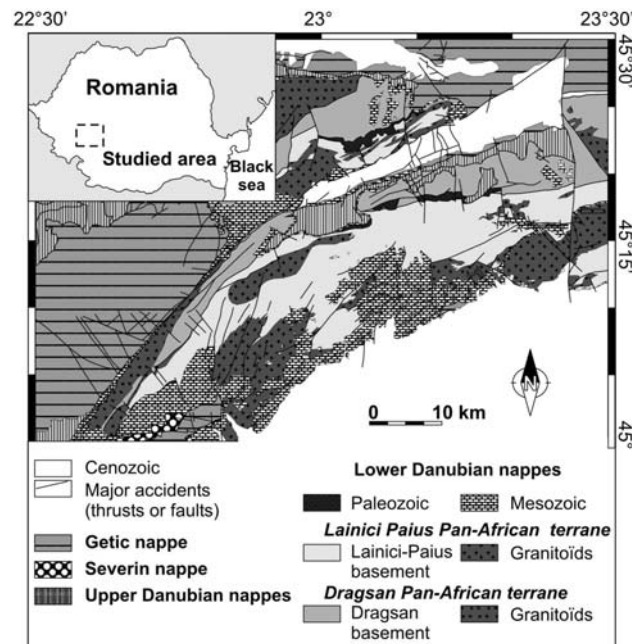


Fig. 1 Simplified geological map of the pre-Alpine units of the South Carpathian Mountains (from the IGR 1:50,000 maps) modified after Berza et al. (1994) and Féménias et al. (2004)

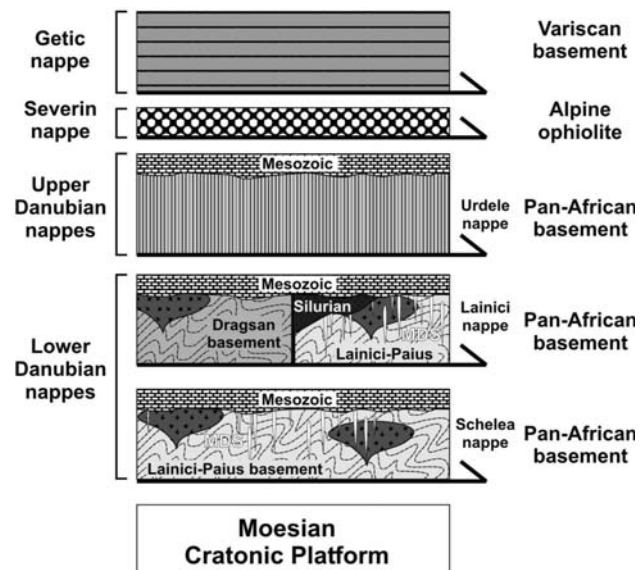


Fig. 2 Schematic cross-section of the Alpine Danubian nappe system in the Southern Carpathians of Romania. In the Lower Danubian nappes, the Motru Dyke Swarm (MDS) crosscuts the Pan-African basement and granitoids of the Lainici-Păiuș basement in the Lainici and Schela nappes. In the Lainici Alpine nappe, the MDS is covered by (Upper Ordovician?) Silurian sediments

et al. 1983, 1994) on the basis of their Mesozoic cover (Stănoiu 1973; Krätner et al. 1981). The Lower Danubian nappes of Lainici and Schela-Petreanu (Krätner et al. 1981, 1988; Berza et al. 1994) contain the same basement

lithologies (Berza and Seghedi 1983). They consist of two Pan-African terranes (Liégeois et al. 1996): the Lainici-Păiuș (Manolescu 1937) migmatitic unit and the Drăgșan (Pavelescu 1953) amphibolitic unit, intruded by several post-metamorphic granitoid plutons and covered by Upper Ordovician-Devonian sediments. The tectonic contact between these two units has been attributed to the Variscan orogeny (Berza and Iancu 1994). The Lainici-Păiuș unit is essentially composed of quartzite, biotite gneiss, marble, graphitic gneiss and leucogranitic bodies, dykes and sills that form an important migmatitic complex showing Pan-African ductile deformation. This unit is characteristically affected by an MP–HT amphibolite metamorphism (Savu 1970; Berza 1978). It is intruded by large, elongated, calc-alkaline to shoshonitic plutons (i.e. the Tismana pluton dated at 567 ± 3 Ma, Liégeois et al. 1996; Duchesne et al. 1998) and by the high-K, calc-alkaline Motru Dyke Swarm (MDS; Berza and Seghedi 1975; recently revisited by Féménias 2003).

The Motru Dyke Swarm (MDS)

This swarm represents the last magmatic event of the area; locally, Silurian sediments cover it. Contrary to leucogranitic dykes, the andesitic to rhyolitic dykes (and sills) of the swarm crosscut the late-precambrian post-collisional plutons (Fig. 2). The MDS intrudes the Lainici-Păiuș basement at a relatively high crustal level. Structures and lithologies of the MDS are exceptionally well preserved, the Alpine deformation being only marked by the development of chlorite along decametre- to metre-spaced joints (lack of a penetrative cleavage). The dykes of the swarm are not uniformly distributed in the studied area. The density distribution of the dykes is also quite variable; some high-density areas have been named (Fig. 3) using the local toponymy. Generally, the high-density large field dykes are sub-parallel, following the main structural trends of the Danubian domain. In a given area, two distinct populations of dykes have been identified (Féménias et al. 2004) on the basis of their size, mean orientation and magnetic fabric: (1) narrow dykes (<1 m) with an 80°N mean wall direction and a symmetrical AMS (anisotropy of magnetic susceptibility) fabric; (2) thicker dykes (>1 m to several metres) with an N-S mean wall direction and an asymmetrical AMS fabric. The two populations have been related to a common regional stress field during a continuum of brittle emplacement (Féménias et al. 2004).

Analytical methods

During a regional survey of the MDS in a mountainous area of 2,000 km², some 150 dykes have been sampled.

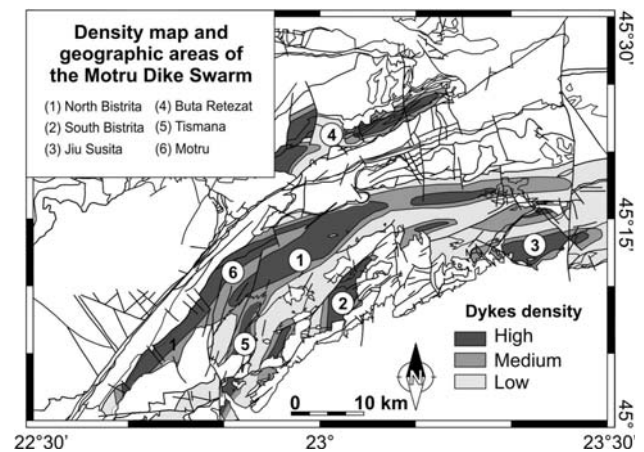


Fig. 3 Relative distribution of the dykes of the Motru Dyke Swarm into the Lainici-Păiuș basement (after Féménias et al. 2004) and location of the cited areas

Detailed petrological, mineralogical and geochemical investigations have been performed on a representative selection of 54 samples.

Major element compositions of the main mineral phases have been determined by WDS electron microprobe (Cameca SX50) at the “Centre d’Analyses par Microsonde en Sciences de la Terre (CAMST, University of Louvain-la-Neuve)”, using a combination of natural and synthetic mineral standards. Operating conditions were as follows: accelerating voltage of 15 kV; beam current of 20 nA; counting time of 10 s for Fe, Mn, Ti and Cr, 16 s for Si, Al, K and Mg and 24 s for Na.

The samples selected for whole rock major and trace element compositions were crushed and ground in a stainless steel mortar. Whole-rock X-ray fluorescence (XRF) spectrometric analyses of major elements and of Cr were made on fused glass discs at the University of Liège (Collectif de Géochimie instrumentale). Some trace elements (Ni, Cu, Zn, V and Sr) were measured by X-ray fluorescence spectrometry on pressed powder pellets (Bologna and Duchesne 1991). Other trace elements (Rb, Cs, Ba, Zr, Hf, Nb, Ta, U, Th, Pb, Y and the rare earth elements, REEs) were analysed by ICP-MS, also at the “Collectif de Géochimie instrumentale”, using the analytical procedure described by Vander Auwera et al. (1998) and detailed in Féménias et al. (2003). The whole-rock geochemical data are reported in Table 1.

Petrography and mineral chemistry

Petrography

The MDS is essentially composed of aphyric to porphyritic basaltic andesites and basaltic trachyandesites, andesites

Table 1 Bulk rock major and trace analyses (XRF and ICP-MS) of representative samples from the Motru Dyke Swarm

Area	Jiu Susita						Tismana						Buta Retezat								
	Sample	R619	R647	R648	R652	R652	R541	R542	R543	R544	R545	R546	R546B	R547	R548	R549	R603	R661	R666	R668	R671
Major element wt%																					
SiO ₂	71.83	57.06	57.95	56.90	49.54	55.19	52.32	52.10	54.18	55.80	58.03	58.17	57.48	52.33	70.16	69.91	70.53	66.35	69.93		
TiO ₂	0.30	0.94	0.93	0.92	1.73	0.85	0.96	0.95	0.92	0.87	0.79	0.78	0.78	0.97	0.34	0.42	0.35	0.61	0.43		
Al ₂ O ₃	14.92	16.71	16.88	15.86	17.17	15.69	15.11	14.97	15.61	15.55	15.23	15.34	14.96	15.27	15.78	15.87	15.73	16.73	15.68		
Fe ₂ O _{3t}	2.52	7.74	6.62	7.43	10.89	7.66	8.58	8.43	8.19	7.60	7.06	6.79	7.01	8.65	3.02	2.96	2.36	4.35	2.85		
MnO	0.07	0.15	0.15	0.09	0.19	0.16	0.15	0.16	0.15	0.15	0.12	0.13	0.12	0.18	0.06	0.05	0.05	0.10	0.06		
MgO	0.61	7.15	6.24	7.24	6.73	10.75	10.55	10.60	8.09	6.74	7.46	7.14	7.28	10.17	1.11	1.22	0.98	2.12	1.21		
CaO	2.16	4.82	5.49	6.10	7.89	5.49	7.12	6.94	7.43	6.19	6.09	6.18	5.83	7.12	1.72	3.02	2.85	2.91	3.04		
Na ₂ O	3.86	3.92	4.25	2.95	3.35	3.12	2.73	2.74	3.32	4.57	3.48	3.71	3.40	3.06	5.43	4.57	4.71	4.44	4.14		
K ₂ O	3.29	1.57	1.54	2.03	2.30	1.35	2.12	2.20	2.16	2.65	2.09	2.09	2.38	1.91	2.63	2.72	2.60	2.93	2.98		
P ₂ O ₅	0.08	0.18	0.17	0.27	0.87	0.15	0.40	0.38	0.20	0.18	0.15	0.16	0.16	0.34	0.10	0.09	0.09	0.18	0.10		
Sum	99.66	100.24	100.22	99.80	100.66	100.41	100.04	99.46	100.25	100.31	100.51	100.49	99.41	100.00	100.36	100.83	100.27	100.72	100.42		
LOI	3.01	2.60	2.13	3.14	2.06	4.59	3.29	3.29	3.08	1.68	3.09	2.98	3.00	3.72	1.59	1.25	1.66	2.17	1.37		
Trace element ppm																					
V	28	96	77	106	146	111	157	142	162	154	132	130	127	147	28	43	37	54	44		
Cr	10	258	195	291	41	426	562	597	365	422	360	322	354	489	11	10	10	10	17		
Co	1	33	34	39	41	47	42	48	40	36	37	36	32	40	10	9	9	17	10		
Ni	<	105	81	114	47	49	249	268	44	34	52	49	50	234	<	<	<	<	1		
Cu	1	10	26	47	31	17	44	31	19	17	17	13	10	42	5	1	1	1	1		
Zn	27	111	88	41	106	71	80	76	68	65	64	59	65	75	54	48	49	69	40		
Ga	17	17	17	16	19	16	16	16	16	14	18	16	17	16	18	18	18	20	18		
Rb	143	73	68	119	96	88	107	123	106	93	99	95	102	120	150	91	76	80	89		
Sr	197	281	345	233	717	255	344	316	365	433	369	359	362	322	272	306	383	515	350		
Ba	688	109	156	203	948	270	565	503	301	683	458	422	567	417	505	402	413	470	426		
Zr	176	161	164	189	244	141	179	171	146	155	173	170	164	167	210	145	147	170	164		
Nb	8	5	4	14	62	7	15	15	11	12	11	11	11	14	11	9	9	10	10		
Th	7.9	2.0	3.8	4.5	6.1	1.1	6.4	6.5	4.3	7.7	11.7	11.8	9.6	5.9	9.4	11.6	9.7	7.8	12.4		
Y	16	19	19	22	33	18	21	20	21	21	21	21	20	21	13	13	8	15	12		

Table 1 continued

Area	Tismana		Motru																
	92R13	92R10	92R11F	92R11G	92R6	92R7	92R8	R522	R524	R553	R563	R567	R569	R570	R571				
Major element wt%																			
SiO ₂	63.22	60.96	58.49	62.83	65.71	65.61	63.00	64.21	52.40	60.78	61.32	54.11	52.61	56.48	52.37				
TiO ₂	0.75	0.77	0.99	0.71	0.49	0.54	0.71	0.62	1.05	0.80	0.72	0.85	0.88	0.94	1.03				
Al ₂ O ₃	16.26	17.48	16.44	15.87	15.76	15.42	16.27	17.10	17.22	17.87	17.80	16.47	14.33	16.93	16.51				
Fe ₂ O _{3t}	5.17	5.84	6.91	5.12	3.91	4.24	4.92	5.11	9.79	5.90	5.87	8.68	8.81	8.13	8.86				
MnO	0.08	0.10	0.10	0.09	0.07	0.07	0.08	0.12	0.15	0.06	0.12	0.17	0.13	0.13	0.14				
MgO	1.55	2.25	2.18	1.63	1.38	1.47	2.12	2.80	5.10	2.62	2.54	8.39	9.66	6.95	8.67				
CaO	5.23	5.58	6.41	5.15	4.02	3.55	4.84	2.83	7.85	3.94	5.31	6.52	8.43	5.31	6.21				
Na ₂ O	4.32	3.96	3.71	4.42	4.29	4.55	4.66	5.13	3.11	2.52	4.37	3.52	2.54	3.26	3.26				
K ₂ O	2.14	1.86	2.30	2.07	2.56	2.23	2.18	2.79	3.25	4.52	2.29	1.21	2.13	2.02	2.01				
P ₂ O ₅	0.18	0.33	0.24	0.20	0.17	0.18	0.24	0.20	0.32	0.28	0.23	0.19	0.33	0.24	0.17				
Sum	100.75	100.21	99.77	99.80	99.92	99.74	100.79	100.90	100.24	99.30	100.58	100.11	99.85	100.39	99.22				
LOI	1.85	1.08	2.00	1.71	1.56	1.88	1.77	1.69	2.89	2.20	1.91	4.28	4.73	2.67	3.05				
Trace element ppm																			
V	-	-	-	-	-	-	-	77	196	61	72	147	173	146	160				
Cr	-	-	-	-	-	-	-	20	58	12	83	344	560	274	376				
Co	7	9	16	5	7	8	8	20	31	18	21	39	39	33	40				
Ni	-	-	-	-	-	-	-	1	9	3	4	121	114	96	142				
Cu	-	-	-	-	-	-	-	3	16	6	7	14	38	30	53				
Zn	-	-	-	-	-	-	-	73	111	65	71	94	91	82	87				
Ga	18	18	19	19	15	18	19	20	19	21	22	18	15	20	19				
Rb	42	63	48	42	74	69	59	98	155	148	71	43	85	69	69				
Sr	707	793	773	721	522	516	616	535	1171	925	744	573	352	487	386				
Ba	522	556	531	533	567	618	602	460	317	985	525	272	243	341	351				
Zr	146	197	132	153	148	172	196	170	144	202	203	144	147	175	147				
Nb	7	13	7	7	11	14	13	11	8	11	12	9	8	10	8				
Th	4.5	6.7	3.6	5.0	14.0	12.4	10.2	10.0	5.5	9.2	9.5	3.6	7.8	4.2	3.2				
Y	18	12	22	20	13	13	12	17	28	21	20	21	21	20	19				
Cs	0.81	1.55	1.01	0.79	0.98	1.21	1.28	1.10	1.58	3.48	1.34	0.92	1.54	1.33	-				
Hf	3.87	5.02	3.73	4.01	4.29	4.24	4.50	4.56	3.93	5.03	4.75	3.57	3.62	4.49	-				
Ta	0.47	0.74	0.51	0.50	0.84	0.90	0.72	0.67	1.17	0.62	0.78	0.54	0.45	0.61	-				
Mo	-	-	-	-	-	-	-	0.51	0.30	0.82	2.02	0.60	1.35	0.93	-				
W	-	-	-	-	-	-	-	3.14	0.20	1.93	0.93	0.85	0.65	0.52	-				

Table 1 continued

Sample	N Bistritia										S Bistritia									
	R533	R620	R622	R623	R624	R632	R633	R635	R637	TJ31	R587	R589	R590	R591	R592	R594	R595	R597	R598	R601
Trace element ppm																				
V	87	140	137	92	166	162	69	166	181	153	44	36	92	47	147	26	43	34	46	54
Cr	42	323	89	92	434	572	67	311	575	527	25	28	11	17	417	10	30	22	92	38
Co	20	35	26	41	35	39	25	34	44	43	9	3	24	4	37	3	8	1	17	14
Ni	1	119	1	76	93	122	6	116	205	164	<	1	1	<	130	<	<	2	60	19
Cu	19	22	7	13	34	9	11	6	54	44	7	1	32	1	30	1	1	1	1	2
Zn	58	97	56	76	72	75	52	82	77	72	43	31	100	36	100	40	33	30	43	39
Ga	18	17	20	16	18	17	21	18	15	14	16	16	22	17	20	18	17	17	17	19
Rb	90	121	57	40	65	84	63	78	94	110	44	59	100	53	69	47	42	52	51	40
Sr	352	313	488	401	454	275	144	369	369	289	329	327	584	418	934	373	398	376	315	442
Ba	323	347	439	133	193	383	539	389	424	560	254	323	179	346	1101	237	129	267	121	235
Zr	154	163	136	172	151	128	290	167	120	125	107	111	229	96	241	101	72	91	107	110
Nb	7	9	9	6	8	7	21	9	17	17	5	5	15	5	18	4	3	4	5	4
Th	6.0	4.9	6.3	1.9	3.9	9.3	8.5	4.6	3.6	5.8	1.5	4.0	7.1	4.8	14.8	3.3	2.0	3.6	4.3	4.0
Y	16	22	18	22	19	19	21	21	21	22	10	11	20	10	27	10	9	8	11	10
Cs	-	0.86	0.78	-	-	0.81	0.57	0.58	-	0.68	-	0.66	0.71	1.36	0.52	1.39	1.20	1.10	-	1.59
Hf	-	4.59	3.42	-	-	3.22	6.70	4.59	-	3.42	-	2.93	5.36	2.67	5.26	2.95	1.89	2.27	-	3.08
Ta	-	0.51	0.59	-	-	0.73	1.16	0.45	-	1.02	-	0.26	0.87	0.33	0.92	0.33	0.18	0.20	-	0.28
Mo	-	1.40	1.15	-	-	0.60	1.21	0.30	-	1.10	-	0.48	1.26	0.17	5.50	0.53	0.32	0.50	-	0.48
W	-	1.10	0.84	-	-	0.20	3.02	0.30	-	0.00	-	2.37	0.88	0.52	0.63	0.86	0.10	1.76	-	1.45
Sn	-	5.20	23.29	-	-	13.80	8.45	13.60	-	2.70	-	7.48	6.25	8.52	34.52	36.35	4.02	3.39	-	3.93
Pb	-	13.27	7.99	-	-	1.98	2.25	3.96	-	3.92	-	7.20	13.44	9.58	6.66	10.49	9.50	9.25	-	8.14
U	-	1.05	2.24	-	-	2.42	2.08	0.98	-	1.42	-	1.16	1.14	1.41	3.52	1.21	0.70	1.43	-	1.01
La	-	30.52	25.94	-	-	43.08	53.90	27.60	-	41.53	-	17.50	38.13	16.90	85.80	15.50	10.40	14.50	-	12.60
Ce	-	48.75	45.06	-	-	78.94	99.90	49.80	-	67.33	-	29.50	75.76	27.68	163.60	25.70	14.30	24.30	-	29.12
Pr	-	6.65	5.22	-	-	10.32	12.10	6.63	-	8.06	-	3.58	8.70	2.79	19.57	3.61	1.77	2.86	-	3.08
Nd	-	24.80	18.76	-	-	37.09	38.33	23.93	-	26.28	-	12.63	34.12	10.07	72.55	12.04	7.42	9.94	-	11.93
Sm	-	5.36	3.67	-	-	7.48	6.81	5.03	-	4.53	-	2.54	6.16	1.91	12.49	2.39	1.58	1.78	-	2.35
Eu	-	1.45	1.17	-	-	1.98	1.75	1.48	-	1.22	-	0.59	1.71	0.69	3.35	0.63	0.58	0.59	-	0.71
Gd	-	4.71	3.48	-	-	5.33	4.91	4.47	-	4.21	-	2.04	4.44	1.91	8.27	2.22	1.52	1.74	-	2.13
Tb	-	0.65	0.54	-	-	0.71	0.73	0.67	-	0.61	-	0.32	0.62	0.30	1.13	0.36	0.23	0.26	-	0.31
Dy	-	3.63	3.18	-	-	3.25	4.13	3.95	-	3.70	-	1.88	3.66	1.62	5.31	2.02	1.45	1.46	-	1.80
Ho	-	0.76	0.63	-	-	0.64	0.80	0.80	-	0.79	-	0.38	0.72	0.34	0.95	0.37	0.28	0.29	-	0.37
Er	-	2.24	1.69	-	-	1.77	2.07	2.24	-	2.12	-	1.06	1.76	0.91	2.17	1.07	0.77	0.80	-	1.06

Table 1 continued

Area	S Bistrita																			
	R533	R620	R622	R623	R624	R632	R633	R635	R637	TJ31										
Sample	R533	R620	R622	R623	R624	R632	R633	R635	R637	TJ31	R587	R589	R590	R591	R592	R594	R595	R597	R598	R601
Tm	-	0.35	0.24	-	-	0.28	0.31	0.32	-	0.32	-	0.16	0.27	0.14	0.31	0.15	0.10	0.12	-	0.16
Y'b	-	2.36	1.73	-	-	1.86	1.85	2.05	-	1.95	-	1.00	1.68	0.90	2.16	0.98	0.69	0.69	-	0.95
Lu	-	0.35	0.25	-	-	0.27	0.26	0.28	-	0.27	-	0.15	0.24	0.13	0.34	0.14	0.09	0.10	-	0.13

Samples 92R13, 92R10, 92R11F, 92R11G, 92R6, 92R7 and 92R8 came from Duchesne (1997)

and dacites; rhyolites and alkali-enriched lithologies (i.e. trachyandesites and trachydacites s.s.) are less common (Fig. 4: TAS classification according to Le Bas et al. 1986; Le Maitre 2002). The dykes have typical chilled margins implying a high level (subvolcanic) emplacement and a flow structure marked by crystal size distribution (CSD; Nkono et al. 2006), shape preferred orientation (SPD) of plagioclase and/or amphibole phenocrysts and/or anisotropy of magnetic susceptibility (AMS; Féménias et al. 2004; Nkono et al. 2006). The variation of the modal proportions of the main phenocrysts during magmatic differentiation of the Motru Dyke Swarm is illustrated in Fig. 5 and discussed below.

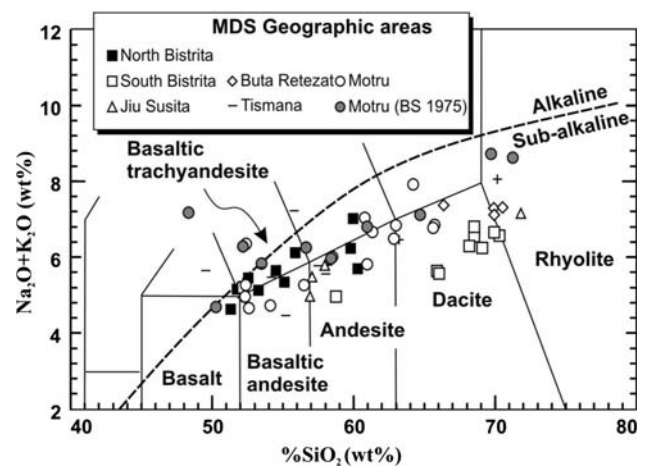


Fig. 4 TAS diagram: whole-rock $\text{Na}_2\text{O} + \text{K}_2\text{O}$ versus SiO_2 (wt%) plot of the dykes of the Motru Dyke Swarm (BS previous data from Berza and Seghedi 1975). Nomenclature domains are from Le Bas et al. (1986); the subalkaline-alkaline boundary is from Irvine and Baragar (1971)

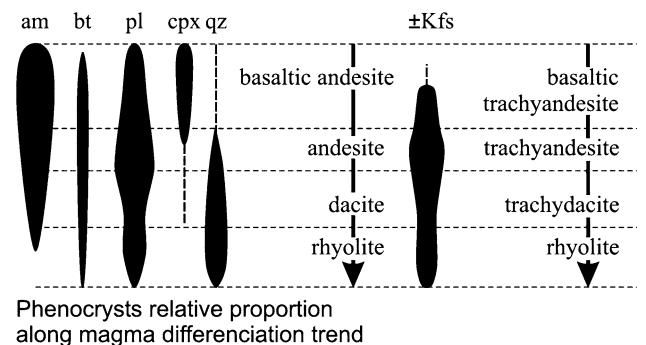


Fig. 5 Sketch diagram illustrating the evolution of the modal proportions of the main phenocrysts during magmatic differentiation of the Motru Dyke Swarm (modified from Féménias et al. 2006). Rocks containing alkali feldspar phenocrysts are relatively rare and characterize the basaltic trachyandesite-trachyandesite-trachydacite-rhyolite series

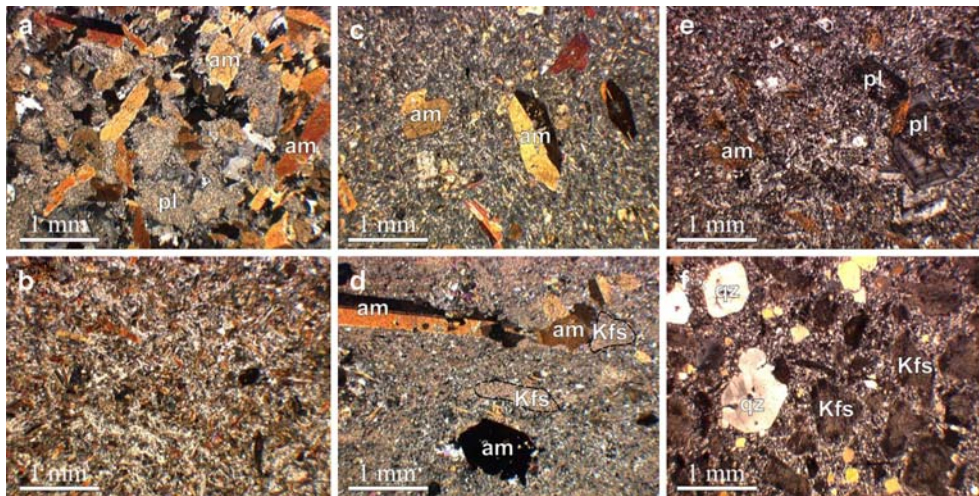


Fig. 6 Microphotographs of some selected dykes of the Motru Dyke Swarm (plane-polarised light) illustrating the main lithologies and textural types. **a** Microcrystalline intersertal fine-grained basaltic andesite characterized by a tangle of amphibole and plagioclase laths. **b** Aphyric basaltic andesite. **c** Typically porphyritic andesite with euhedral amphibole phenocrysts. **d** Porphyritic (amphibole and ghost

alkali feldspar replaced by a white mica-albite association) trachyandesite. **e** Porphyritic dacite with euhedral zoned plagioclase and subhedral to anhedral accessory green amphibole. **f** Phenocryst-rich rhyolite with resorbed euhedral quartz and ghost alkali feldspar replaced by a white mica-albite association

Basaltic andesite

Basaltic andesite is a quite abundant rock by volume in the MDS; it constitutes a majority of the thick dykes (1–30 m). Texture progressively evolves from microcrystalline intersertal (characterized by a tangle of brown amphibole and plagioclase laths) in the core of the dyke (Fig. 6a) to aphyric at the margins of the dyke (Fig. 6b). The rocks are generally fine-grained; a few coarse-grained samples with plagioclase and amphibole crystals of 1–2 mm in length were found. Rare basalts s.s. have been observed, characterized by higher modal proportions of amphibole and clinopyroxene. In all textural types, the euhedral brown amphibole, commonly twinned, is well preserved, whereas the subhedral plagioclase has suffered a strong deuteric alteration and is pseudomorphosed by a white mica + epidote + albite association. The groundmass consists of tiny quartz, plagioclase, ferromagnesian phases (amphibole and rare clinopyroxene), oxides and devitrified glass. Mn-rich ilmenite is the main primary oxide of the MDS.

Basaltic trachyandesites are less common; they look like the basaltic andesites but contain a lower proportion of amphibole (only present in the matrix) and a higher proportion of secondary albite. They display aphyric to glomeroporphyritic textures in agreement with their occurrence as thin dykes (<1 m). The Na-rich primary plagioclase is always albitised. Basaltic trachyandesites have been observed in the Tismana, Motru and North Bistrita areas (Fig. 3).

Andesite

With basaltic andesite, it represents the main lithology of the MDS and is present in the whole studied zone. The texture is typically porphyritic (Fig. 6c) with zoned brown amphibole and/or zoned plagioclase phenocrysts. Euhedral amphibole is fresh. On the contrary, the plagioclase displays a deuteric alteration marked by development of white mica, epidote and albite (localized in the Ca-rich zones) and albitization (localized in the Na-rich zones). Clinopyroxene is rare; some anhedral quartz has been observed. The groundmass is comparable to that of the basaltic andesites. The thin dykes (<1 m) display a good SPO, marked by amphibole and plagioclase phenocrysts. Trachyandesite s.s. (Fig. 6d) is rare (only present in the Tismana, Motru and North Bistrita areas) and petrographically characterized by the presence of ghost alkali feldspar (replaced by a white mica-albite association).

Dacite

It is very fine-grained and shows sub-intersertal to porphyritic textures with plagioclase, accessory green amphibole and resorbed quartz. Plagioclase is euhedral, zoned and rarely altered (Fig. 6e). The amphibole, less common than in mafic lithologies, is a subhedral to euhedral (prismatic or acicular) green hornblende. The groundmass is made of quartz, albite, mica and epidote; it also contains amphibole that is partly transformed to tremolite and chloritized. Some samples are aphyric and

only contain small partly resorbed euhedral quartz. The dacitic dykes appear heterogeneous in the field; they display locally glomero-porphyritic texture (clots of quartz and plagioclase phenocrysts) and are cut by siliceous veinlets. Rare ghost phenocrysts of alkali feldspar (replaced by white mica and albite) characterize the trachydacite sub-facies. Dacite has not been observed in the North Bistrita area; by contrast, it represents the main lithology of the South Bistrita and Jiu areas (see Fig. 3).

Rhyolite

It displays porphyritic (seriate-textured) microcrystalline textures. Quartz and/or alkali feldspar phenocrysts (accessorily plagioclase) can constitute up to half the volume of the rock (Fig. 6f). Quartz occurs as phenocrysts (euhedral with resorption) and/or anhedral to subhedral microcrystals in the groundmass. Some rhyolites contain two feldspars and/or green hornblende (more or less altered in chlorite and/or tremolite), but are often devoid of quartz phenocryst. Rhyolites are heterogeneous, displaying local glomero-porphyritic texture and siliceous veinlets. They occur as dykes (South Bistrita area; Fig. 3) or sills (Buta-Retezat area; Fig. 3) and are less common in the other localities.

Mineral chemistry

Magmatic primary phase assemblage

Calcic-amphibole is a ubiquitous phase in all the MDS rocks; it occurs as phenocryst or as a groundmass phase. It displays a large compositional range, varying from kersutite \rightarrow Ti-pargasite \rightarrow pargasite \rightarrow Ti-magnesiostastingsite \rightarrow magnesiostastingsite \rightarrow edenite \rightarrow tschermakite \rightarrow magnesiohornblende, in the differentiation sequence from basaltic andesite to rhyolite (Féménias et al. 2006). Pargasite-magnesiostastingsite crystals in intermediate rocks display complex zoning and partial resorption; these phenomena have been interpreted in terms of self-organization of oscillatory zoning, without significant heating and/or magma mixing (Féménias et al. 2006). In all rock types, amphibole phenocrysts equilibrated at a nearly constant pressure of about 0.6 ± 0.1 GPa, but their temperature of crystallization ranges from 1,000 to 900°C for basaltic andesites to 700–600°C for dacites. In rhyolites, the amphibole (edenite to magnesiohornblende) records a continuous range of P–T conditions, from 700°C/0.6 GPa to 600°C/0.1 GPa, in agreement with their change of habit from euhedral to subhedral (Féménias et al. 2006). Moreover, the rim of the amphibole phenocrysts was altered during late-emplacement hydrothermal activity.

The zoned plagioclases of dacites and rhyolites are fresh, but the plagioclases of mafic rocks (basaltic andesite

- andesite) are always strongly altered, so that very few microprobe analyses were obtained on rare fresh core areas. To increase the database, plagioclase compositions were tentatively quantified using BSE (Back-Scattered Electrons) images that allow us to estimate the modal proportions of the secondary assemblage albite-epidote-white mica and the composition of these phases. Broadly speaking, the composition of the cores of plagioclase only displays slight variations in the range of An_{33–50}. Moreover, there is no systematic and significant correlation between plagioclase core composition and degree of magmatic differentiation of their host lava. By contrast, the compositional variations observed in oscillatory-zoned phenocrysts of dacites, i.e. An_{28–50} and An_{37–60} for two phenocrysts of one sample, overlap with the variation of the whole differentiation sequence. All the plagioclase microcrystals from the groundmass have an albitic composition (An_{0–5}), resulting from the deuteritic alteration.

Clinopyroxene is present in the basaltic andesites and andesites. It is often altered (chloritization and/or ouralutization). Rare preserved crystals have been observed in chilled margins; they have a diopside to augite composition and a relatively high Mg[#] (Mg[#] = Mg/(Fe + Mg)) of 0.85–0.87.

Microcrystals and phenocrysts of biotite are ubiquitous in the marginal zones of numerous basaltic andesite and andesite dykes. They show a narrow range of composition (Phl_{51–65} Ann_{35–40} Sid_{0–12}) and have low Fe[#] (Fe[#] = Fe/(Fe + Mg)) values, between 0.34 and 0.43. Using the experimental fO_2 –T–Fe[#] relationship of Wones and Eugster (1965), these compositions correspond to high-T micas, around 900°C for QFM buffer conditions.

Mn-rich ilmenite (Il_{85–91}Ge_{0.3–0.7}Py_{9–14}) is the main oxide; it is prismatic in the core of the dyke and anhedral and/or acicular near the walls. Comparable manganian ilmenite has been observed by Snetsinger (1969) in the Sierra Nevada adamellite.

Rare spinel (Mg–Al chromite) has been found in the mafic dykes.

Deuteritic and propylitic secondary phase assemblage

The MDS rocks have been retrogressed by deuteritic alteration and propylitization processes that occurred during (pseudomorphs deformed during flowing) and/or just after (shape pseudomorphs not affected by flowing) dyke emplacement. These processes led to low-temperature, low-pressure secondary paragenesis. The primary Ti-bearing silicate phases (amphibole and biotite) were transformed to leucoxene. Secondary chlorite, calcite, talc, epidote and pyrrhotite-pyrite (subsequently altered into goethite and hematite) developed as millimetre-sized euhedral grains in the groundmass or as replacement products

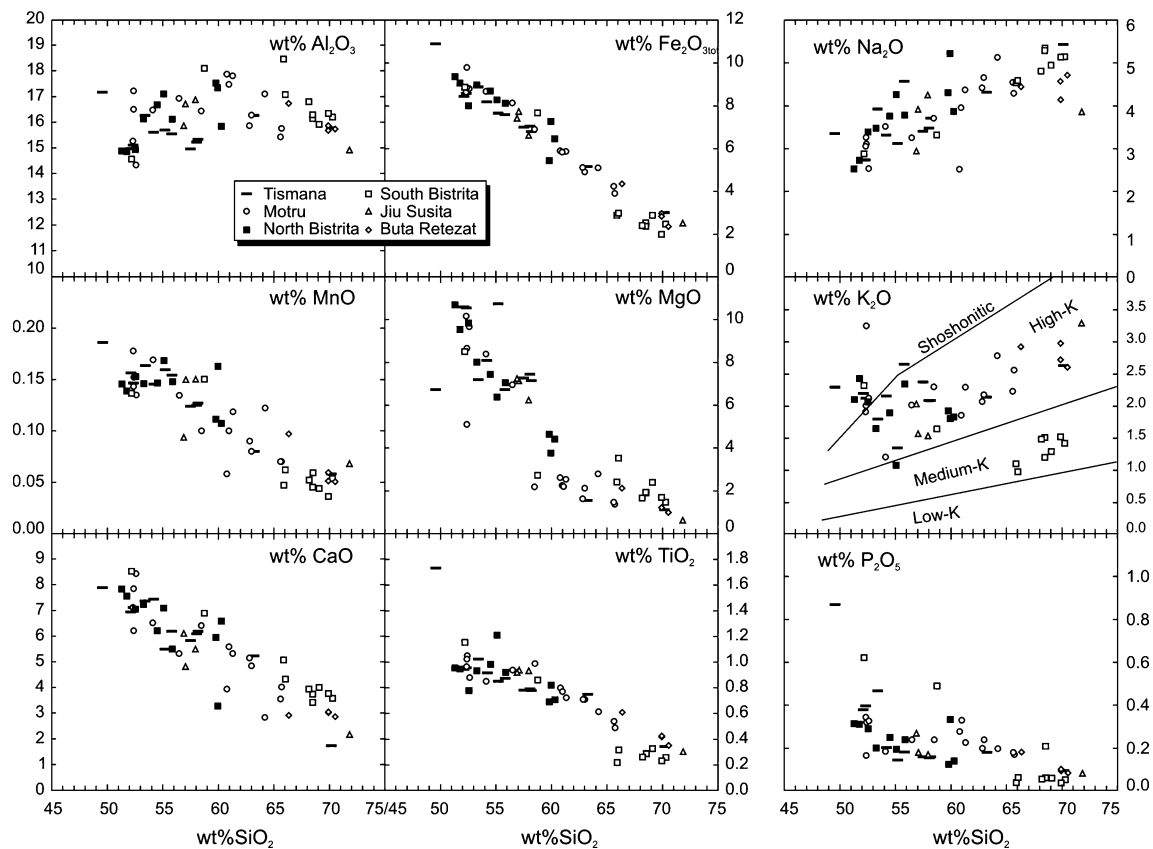


Fig. 7 Major element Harker plots (oxides versus SiO_2 in wt%) for the Motru Dyke Swarm. In the K_2O versus SiO_2 diagram, the domain boundaries are from Rickwood (1989)

of the amphibole. A pseudomorphic replacement of calcic amphibole phenocrysts by talc suggests a strong propylitic process (Féménias 2003). Alkali feldspar phenocrysts are always replaced by a white mica + albite assemblage, whereas plagioclase is albitized or transformed to white mica + epidote + albite assemblage. A ferromagnesian chlorite ($0.59 < \text{Mg}^\# < 0.71$) replaces the clinopyroxene phenocrysts; a second chlorite (with comparable $\text{Mg}^\#$, but lower Cr and Ca content) occurs in the matrix. Using the chlorite solid solution geothermometer developed by Cathelineau and Nieva (1985) for ferromagnesian chlorites from the Los Azufres (Mexico) hydrothermal system, the P–T conditions during the alteration of the MDS rocks were estimated at $T = 200\text{--}260^\circ\text{C}$ for $P \sim 0.1$ GPa. These values are in agreement with a sub-surface hydrothermal activity that was probably coupled to an aerial volcanic activity.

The groundmass has recrystallized to a microcrystalline assemblage dominated by epidote, albite, quartz and white mica (compositions varying between phengite and muscovite). Epidote ($\text{Ca}_{1.97\text{--}2.07} \text{Fe}_{0.7\text{--}0.83}^{3+} \text{Fe}_{0.02\text{--}0.0}^{2+} \text{Al}_{2.1\text{--}2.2} \text{Si}_{3\text{--}3.15} \text{O}_{12}(\text{OH})$) also occurs with calcite and apatite in millimetre-sized bubble-shaped areas. Locally, at

the contact with quartz, they display lower Fe content and higher Si and Al content; the composition evolves to a prehnite.

Geochemical results

Whole-rock major elements

A total of 54 whole-rock analyses of sub-volcanic rocks from the main geographic areas of the Motru Dyke Swarm are listed in Table 1 and plotted together with ten analyses from Berza and Seghedi (1975) in the total alkali versus silica classification (TAS) diagram of Le Maitre (2002), used for volcanic rock nomenclature (Fig. 4). Major element compositions (normalized to 100% on a volatile-free basis) are plotted on Harker-type diagrams (Fig. 7). As illustrated in the petrographic section, the Motru Dyke Swarm is characterized by a complete chemical sequence of lava composition from basaltic andesite to rhyolite, that is from ~ 50 up to 71.8 wt% SiO_2 , respectively. Basaltic andesites and andesites (52–63 wt% SiO_2) are largely predominant (Fig. 4). The Motru Dyke Swarm magmatic suite

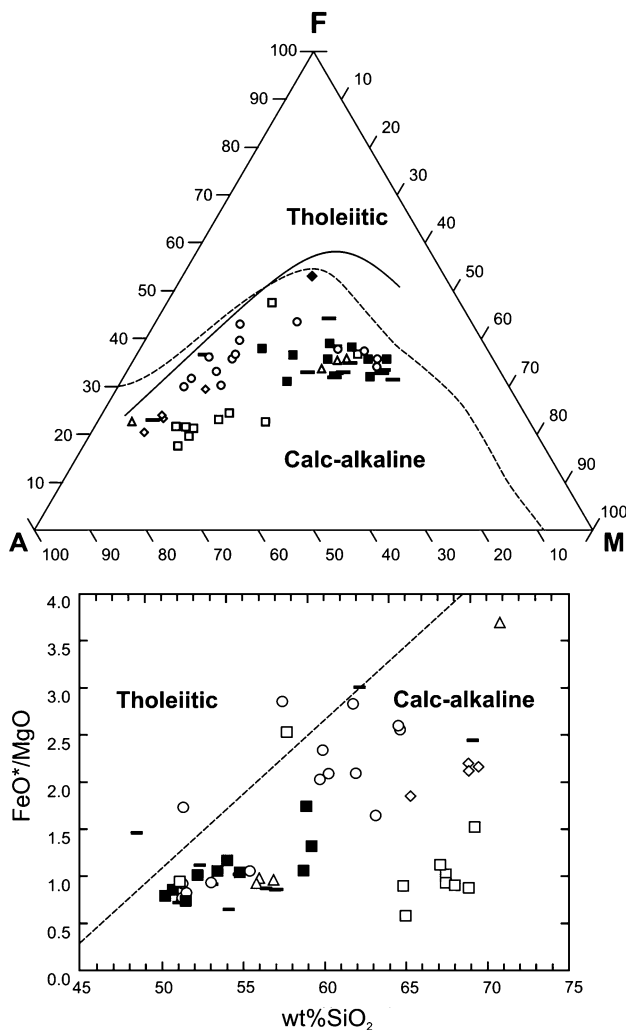


Fig. 8 Whole-rock calc-alkaline affinity of the Motru Dyke Swarm. **a** AFM ($\text{Na}_2\text{O} + \text{K}_2\text{O}$; FeO , MgO in wt%) diagram, domain boundaries are from Kuno (1968, *hard line*) and Irvine and Baragar (1971, *dotted line*); **b** FeO^*/MgO versus SiO_2 (wt%) diagram (FeO^* is total Fe expressed as FeO), the tholeiitic-calc-alkaline dividing line is from Miyashiro (1974). Symbols as in Fig. 3

is clearly sub-alkaline (Fig. 4) with a clear calc-alkaline affinity, as shown in the AFM and FeO^*/MgO versus SiO_2 diagrams (Fig. 8). Three rocks from this study and two additional rocks from Berza and Seghedi (1975) fall barely in the alkaline field. Shoshonitic to high-K basaltic andesites and high-K andesites, dacites and rhyolites have been found in all the field areas, while coeval dykes from the South Bistrita area are almost exclusively medium-K dacites and rhyolites (Fig. 7). Although the syn-emplacement alteration could partially account for the dispersion of the data for K_2O , Na_2O and P_2O_5 contents, the variations in K_2O and Na_2O contents are clearly correlated with the variations in the modal abundance of magmatic alkali feldspar in thin section. In most Harker diagrams (except K_2O), the MDS rocks display a broad common evolution

trend, with no clear distinctions between the various areas, except for the dominant lithology, which is basaltic andesite in the North Bistrita and dacite in the South Bistrita area. Broadly speaking, Na_2O and K_2O increase with SiO_2 , whereas Al_2O_3 , MnO and P_2O_5 show, respectively, roughly convex upward, flat or slight decreases. Total iron (as Fe_2O_3), CaO , MgO and TiO_2 decrease significantly with increasing SiO_2 content. The samples do not plot along a well-defined evolution line; the apparent scatter obviously reflects the mobility of this element during deutritization of some samples and variation of the modal proportion of phenocrysts (mainly plagioclase; locally alkali feldspar), from sample to sample. Some samples are indeed strongly porphyritic, while others are almost aphyric. The roughly convex upward profile of Al_2O_3 versus SiO_2 allows us to discriminate rocks in which mafic phenocrysts (amphibole and/or clinopyroxene) are predominant from those that have felsic phenocrysts (plagioclase and/or K feldspar), the limit is at ~ 60 wt% SiO_2 . Such major element trends are broadly consistent with fractionation of the observed phenocryst phases from a basaltic andesite and/or basalt parent. The composition of these parental magmas did not vary significantly between areas (or over time?), except maybe for a significant decrease in potassium in the South Bistrita area.

Whole-rock trace elements

The trace element compositions of the various MDS rocks are plotted on multi-element diagrams (Fig. 9, normalization to the composition of Pyrolite = primitive mantle) and on chondrite-normalized REE diagrams (Fig. 10, normalizing values from McDonough and Sun 1995). As the rocks from the different regional zones broadly follow the same evolution trends in Harker diagrams, the trace element diagrams are not displayed according to geographic areas, but instead using the petrographical-chemical classification, which is in fact the SiO_2 content. The Motru rocks are compared to the classical low-K to shoshonitic calc-alkaline lava suites worldwide: the low- to medium-K calc-alkaline suite is illustrated by the Montserrat volcanic series (data from Zellmer et al. 2003), the medium- to high-K suite by the Cainozoic Central Andes (data from Richards and Villeneuve 2002) and the high-K to shoshonitic suite by the Tibet volcanic series (data from Miller et al. 1999). All samples, whatever their degree of evolution, are enriched in LILE, Pb and LREE and relatively depleted in Nb, Ta, P and Ti, which is a typical feature of arc-related magmas worldwide (e.g. Gill 1981; Pearce 1982; Pearce and Peate 1995). In the calc-alkaline series used for comparison, the degree of incompatible element enrichment and the REEs

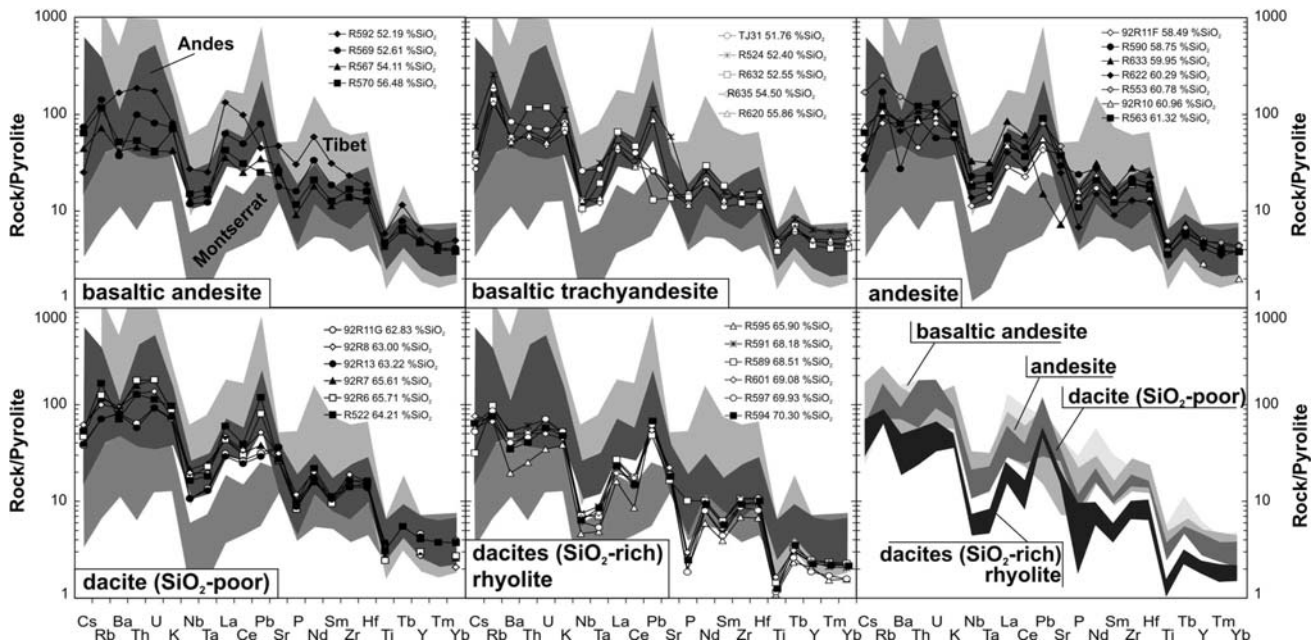


Fig. 9 Pyrolite-normalized multi-element variation diagrams for the whole-rock samples from the MDS. Normalizing values from McDonough and Sun (1995). Comparison with the shoshonitic to high-K calc-alkaline rocks from Tibet (Miller et al. 1999), medium-

to high-K calc-alkaline lavas from Central Andes (Richards and Villeneuve 2002) and medium- to low-K calc-alkaline lavas from Montserrat (Zellmer et al. 2003)

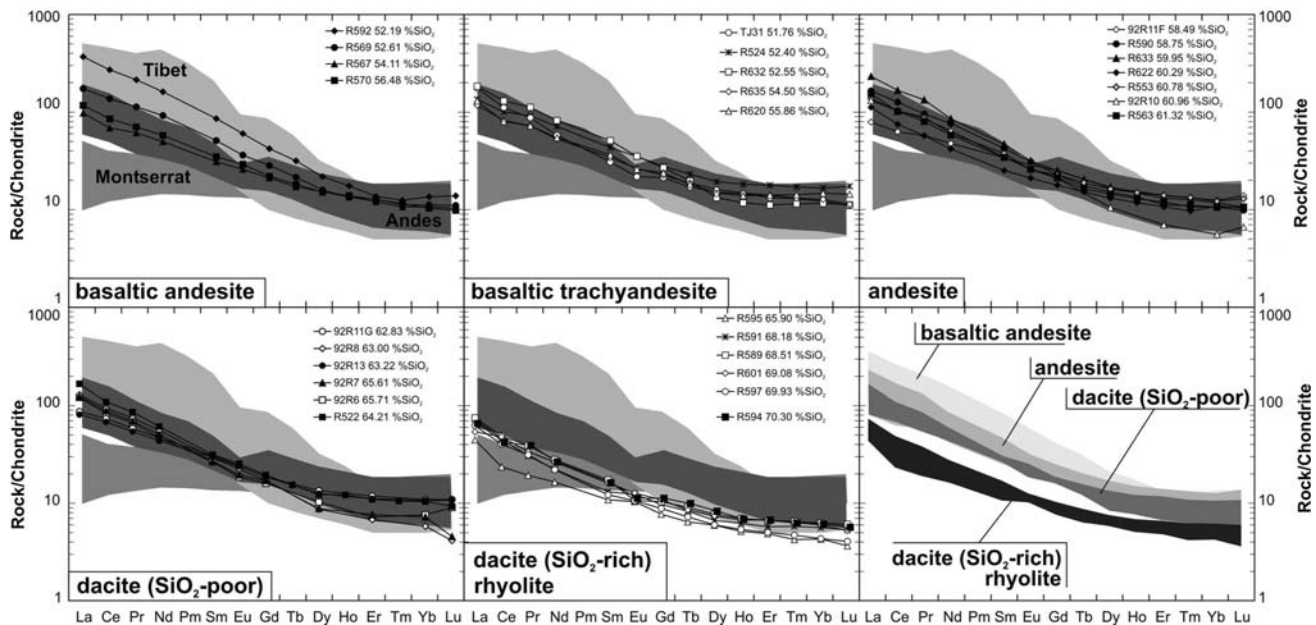


Fig. 10 Chondrite-normalized REE patterns for whole-rock samples from the MDS. Normalizing values from McDonough and Sun (1995). Comparison with the shoshonitic to high-K calc-alkaline rocks from Tibet (Miller et al. 1999), medium- to high-K calc-

alkaline lavas from Central Andes (Richards and Villeneuve 2002) and medium- to low-K calc-alkaline lavas from Montserrat (Zellmer et al. 2003)

and trace element content appear strongly correlated to the K content of the suites, and by extension to the crustal thickness. In that sense, the medium- to high-K Motru

Dyke Swarm patterns are logically closer to the medium- to high-K Cainozoic Central Andes volcanic suite than to the low- to medium-K Montserrat suite. Independently of

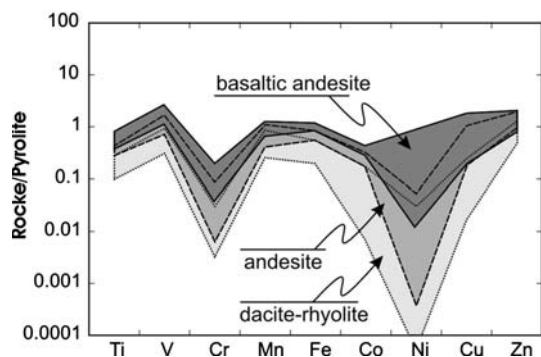


Fig. 11 Pyrolite-normalized transition element variation diagrams for the whole-rock samples of the MDS. Normalizing values from McDonough and Sun (1995)

the rock types, the REE patterns are all characterized by LREE enrichment ($La_N/Yb_N = 6.3\text{--}27.0$; $La_N/Sm_N = 2.3\text{--}5.7$) and by no or only slightly negative Eu anomalies ($Eu_N/Eu^* = 0.8\text{--}1.1$). The range of LREE enrichment is wider than those of the medium- to high-K Cainozoic central Andes volcanic suites; it is similar to volcanic suites related to subduction zones with thin continental crust ($6 < La_N/Yb_N < 27$; Kay et al. 1991) for which magmatic processes do not involve garnet fractionation. The trace elements contents (including REE) significantly decrease with increasing SiO_2 content (Figs. 9, 10). The mafic and intermediate volcanics (basaltic andesites and andesites) have the highest trace element content, in particular, the highest REE ($\Sigma REE = 103\text{--}228$ ppm with the basaltic andesite R592: 378 ppm). The trace element content in dacites and rhyolites are distinctly lower ($\Sigma REE = 41\text{--}156$ ppm), but the patterns remain similar. Some elements (U, Th and Pb) do not show any evolution trend. Others (Ba, Ga, Sr, Zr and Hf) display trends

comparable to Al_2O_3 (Fig. 7), which probably results from the change of the modal proportions of the fractionating assemblage. When the complete set of data (54 samples) is observed, it appears that all the transition element (major and minor) contents systematically decrease during differentiation (Fig. 11); the negative Cr and Ni anomalies become deeper from basaltic andesite to rhyolite, which is also characteristic for calc-alkaline arc-related evolution.

Discussion

Fractional crystallization and magma differentiation

Even if complex processes like crustal melting, assimilation, storage and homogenization (MASH; i.e. Winter 2001) can occur by the underplating of mafic magmas, the systematic variation of the major and trace element contents of the MDS rocks (Figs. 7, 9, 10, 11) can reasonably be interpreted qualitatively in terms of fractional crystallization. This is indicated by the curvilinear trends of some elements in Harker diagrams, especially Fe_2O_3 , CaO and MgO, and by the turnover or change of slopes of the trends of Al_2O_3 versus MgO (Fig. 12), and of Ba, Ga, Sr, Zr and Hf versus SiO_2 . These trends can be related to variations of the modal proportions of the main phases in the fractionating assemblage (Fig. 12). The trends are qualitatively consistent with the fractionation of the main phenocryst phases Ca-amphibole, clinopyroxene and plagioclase. At the beginning of the fractionation process, the Al_2O_3 content increases with increasing SiO_2 (up to 60%; Fig. 7) and decreasing MgO contents (Fig. 12). The Fe_2O_3 , TiO_2 , CaO and MnO (Fig. 7) as well as the transition elements (Fig. 11) contents strongly decrease

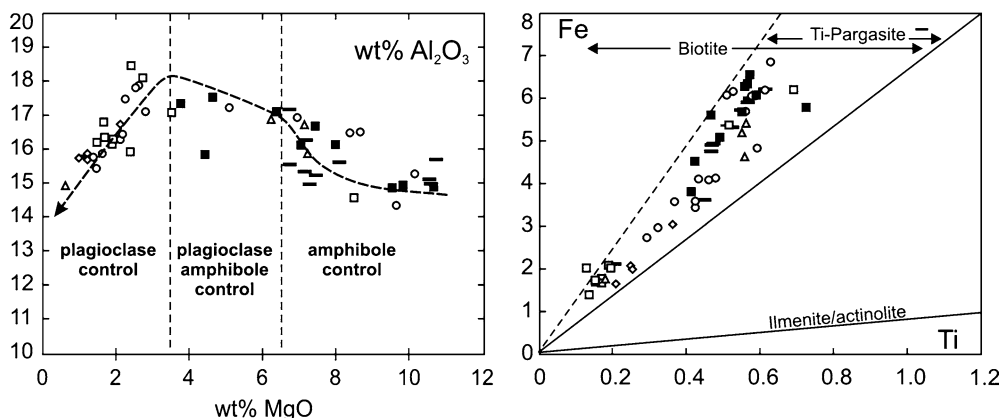


Fig. 12 Al_2O_3 versus MgO (wt%) (a) and Fe versus Ti (wt%) (b) diagrams. Mineral compositions correspond to the data obtained by electron microprobe in the MDS lithologies

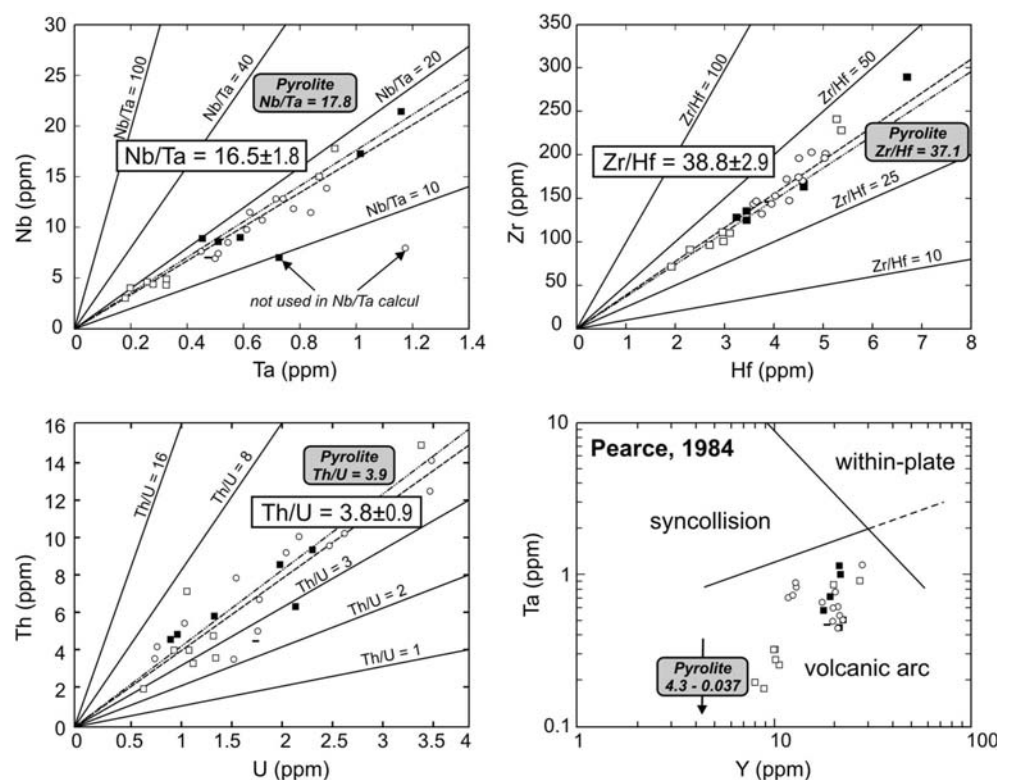
during this stage, which is consistent with the early fractionation of mafic phases (amphibole, clinopyroxene, Mn-ilmenite). Then the Al_2O_3 content strongly decreases with decreasing MgO (Fig. 12) and the LIL elements (Rb, Sr and Ba) also decrease suggesting that plagioclase (\pm K-feldspar in the most alkaline lithologies trachyandesites and trachydacites) is the main fractionating phase. K_2O content versus SiO_2 is complex and scattered involving locally K-feldspar, and especially biotite fractionation (pulses), at different stages of the evolution. As the REE partition coefficients between HT calcic-amphibole and calc-alkaline magma (i.e. Hanson 1980; Sisson 1994; Brenan et al. 1995) are higher than 1 (REEs are compatible in HT calcic-amphibole in calc-alkaline environment), the REE content decreases during the magmatic evolution from the primitive basaltic andesite to the evolved rhyolite. The same behaviour has been observed and modelled in the Dokhan-type volcanic rocks of Egypt (Mohamed et al. 2000). Experimental studies on water-saturated calc-alkaline magma (Grove et al. 2003) have shown that calcic amphibole can be the main ferromagnesian phase in the absence of olivine. But, unlike olivine, amphibole remains on the liquidus all along the crystallization interval, from the early basaltic andesite to the late rhyolites. The amphibole composition varies regularly from Si-poor, Ti-rich kaersutite in the mafic rocks to Si-rich actinolite in the felsic rocks (Féménias et al. 2006).

The Ti-pargasite, which is the common phenocryst in the Motru rocks, controls the Ti/Fe ratio of the whole magma series (Fig. 12). There is no significant difference in composition between the small ($< 50\mu\text{m}$) and large (up to $3,000\mu\text{m}$) amphibole grains in a given rock, which excludes the possibility of several generations of crystals. The different amphibole types of the primary magmatic sequence have decreasing crystallization temperature from basalt ($\sim 1,000^\circ\text{C}$) to rhyolite ($\sim 650^\circ\text{C}$). By contrast, pressure estimate for all amphiboles is nearly constant and close to 0.6–0.7 GPa. These P–T conditions imply the existence of monogenic magma chambers in the deep crust (or in the upper mantle, the crust is very thin) and, according to phenocryst zoning, an evolution in a closed system. A single liquid line of descent process thus most probably controls the rocks of the Motru Dyke Swarm. This could be checked by the analyses of glassy melt inclusions trapped by crystallizing phenocrysts (e.g. Devine and Sigurdsson 1983; Rutherford and Devine 1988), but in Palaeozoic volcanic suites like the MDS, these inclusions have probably completely (re)crystallized.

Parental magma, source and tectonic implications

The trace element contents of the MDS rocks regularly decrease (Figs. 9, 10, 11) with increasing differentiation from basaltic andesites to rhyolites. As crustal materials

Fig. 13 Nb-Ta (a), Zr-Hf (b), Th-U (c) and Ta-Y (d) binary diagrams from the Motru Dyke Swarm samples. Ratios are given with $\pm 1\sigma$ error; pyrolite values are from McDonough and Sun (1995). The tectonic fields in the Ta-Y diagram are from Pearce et al. (1984). Symbols as in Fig. 3



generally have higher LIL trace element contents than mantle-derived magmas, this behaviour rules out the contamination of the magma by crustal materials during fractionation, on one hand, and a crustal origin for the rhyolites, on the other hand. The Nb/Ta, Zr/Hf and Th/U ratios remain constant throughout the whole MDS suite (Fig. 13a–c). The calculated average values for these ratios (16.5 ± 1.8 ; 38.8 ± 2.9 and 3.8 ± 0.9 , respectively) are reasonably close to the Pyrolite values (McDonough and Sun 1995) and imply a single mantle source for the parental magma of the MDS suite. The high-K calc-alkaline rocks, in general, and the rocks of the MDS suite, in particular, are characterized by LILE and LREE enrichments, combined with relative depletions in HFSE (Gill 1981; Wilson 1989). These rocks typically display volcanic arc geochemical signature (Peccerillo 1985; Rogers et al. 1985) and have been related to subduction zones; this is also observed for the MDS rocks (Figs. 12, 13). Nevertheless, for old volcanic suites, like the Palaeozoic MDS, the use of the geochemical signature to infer their lost (subduction related? Fig. 11) tectonic settings is hotly debated (e.g., Rock 1984; Zhou 1985; Sloman 1989; Turner et al. 1999; Mohamed et al. 2000; Moghazi 2003). Moreover, emplacement of high-K magmas with typical arc-type trace element signature can post-date active subduction episode and occur synchronously with uplift, extension or strike-slip movement (Rottura et al. 1998; Wang et al. 1999; Sloman 1989). The large difference in the K-content of various calc-alkaline series worldwide has been related to the influence of the variations of crustal thickness during melting processes (see evolution from low-K to shoshonitic suites illustrated in Figs. 9, 10). In that sense, the high-K Motru Dyke Swarm suite could be the geodynamic marker of a thin continental crust that resulted from the late- to post-orogenic extension of the Danubian area. It has been suggested by several authors (e.g., Rogers et al. 1987; Thirwall 1988; Sloman 1989; Féménias et al. 2003) that geochemical features of old calc-alkaline volcanic suites could be related to chemical heterogeneities generated in the mantle during trace element enrichment events (metasomatism), in relation with a subduction episode, and that this enrichment could last for substantial periods of time after cessation of subduction.

Conclusion

- The Pre-Silurian Motru Dyke Swarm (MDS) outcrops in the Alpine Danubian nappes of Southern Carpathians (Romania). It corresponds to a well-preserved sub-volcanic suite emplaced in a late- to post-orogenic

(Pan-African orogeny) tectonic setting. It is heterogeneously distributed on a $\sim 2,000 \text{ km}^2$ area and displays an extended, continuous lithological sequence formed of aphyric to micro-porphyritic basaltic andesite, andesite, dacite and rhyolite.

- The whole suite has a typical high-K calc-alkaline major and trace element geochemical signature that results from the fractional crystallization of a basaltic andesite and/or basalt parent magma; the main observed phenocrysts being amphibole, clinopyroxene and plagioclase.
- The transition and trace element contents (LILE and REE) significantly decrease during differentiation, while the Zr/Hf, Th/U and Nb/Ta ratios are kept constant and close to mantle values. These data argue for a cogenetic relationship between all the lithologies, including rhyolites, and suggest that the mantle-derived magma evolved without significant crustal contamination.
- The petrographical and geochemical data point to a typical “arc-related magma suite”. Nevertheless, like for other Palaeozoic volcanic series, the tectonic setting of the MDS is clearly late- to post-orogenic. This could mean that the melting of an enriched (subduction-related) mantle source occurred quite a long time ago, after the cessation of the subduction itself. The geochemical characteristics of such magmatic series have to be used with caution to infer the tectonic setting during emplacement.

Acknowledgments We gratefully acknowledge the thorough and constructive comments of Dr. Montero and of an anonymous reviewer.

References

- Abdel-Rahman AFM (1995) Tectonic-magmatic stages of shield evolution: the Pan-African belt in northeastern Egypt. *Tectonophysics* 242:223–240. doi:10.1016/0040-1951(94)00171-5
- Abdel-Rahman AFM, Doig R (1987) The Rb-Sr geochronological evolution of the Ras Gharib segment of the northern Nubian shield. *J Geol Soc Lond* 144:577–586
- Aftabi A, Atapour H (2000) Regional aspects of shoshonitic volcanism in Iran. *Episodes* 23:119–125
- Akay E, Erdogan B (2004) Evolution of neogene calc-alkaline to alkaline volcanism in the Aliaga-Foça region (Western Anatolia, Turkey). *J Asian Earth Sci* 24(3):367–387. doi:10.1016/j.jseaes.2004.01.015
- Berza T (1978) Studiul mineralogic și petrografic al masivului granitoid de Tismana. *An Inst Geol Geofiz* LIII:5–176
- Berza T, Iancu V (1994) Variscan events in the basement of the danubian nappes (South Carpathians). In: Berza T (ed) *Geological evolution of the Alpine-Carpathian-Pannonian system, ALCAPA II, field guidebook*, Romanian J Tecton Reg Geol 75:93–104
- Berza T, Seghedi A (1975) Complexul filonian presilurian din bazinul Motrului (Carpatii Meridionali). *D S Inst Geol Geofiz* LXI/1:131–149

- Berza T, Seghedi A (1983) The crystalline basement of the Danubian units in the Central South Carpathians. *An Inst Geol Geofiz LXI*:15–22
- Berza T, Kräutner HG, Dimitrescu R (1983) Nappe structure of the Danubian window of the central South Carpathians. *An Inst Geol Geofiz* 60:31–34
- Berza T, Balintoni I, Iancu V, Seghedi A, Hann HP (1994) South Carpathians. In: Berza T (ed) Geological evolution of the Alpine-Carpathian-Pannonian system, ALCAPA II, field guide-book, Romanian J Tecton Reg Geol 75:37–49
- Bologne G, Duchesne J-C (1991) Analyse des roches silicatées par spectrométrie de fluorescence X: précision et exactitude. *Belg Geol Surv Prof Paper* 249:1–11
- Brenan JM, Shaw HF, Ryerson FJ, Phinney DL (1995) Experimental determination of trace-element partitioning between pargasite and a synthetic hydrous andesitic melt. *Earth Planet Sci Lett* 135(1–4):1–11
- Cathelineau M, Nieva D (1985) A chlorite solid solution geothermometer: The Los Azufres (Mexico) geothermal system. *Contrib Mineral Petrol* 91:235–244. doi:10.1007/BF00413350
- Devine JD, Sigurdsson H (1983) The liquid composition and crystallization history of the 1979 Soufriere magma, St Vincent, WI. *J Volcanol Geotherm Res* 16:1–31. doi:10.1016/0377-0273(83)90082-3
- Duchesne J-C (Ed.) (1997) Geochemistry of Romanian granites. Final report, CIPA programme, Laboratoires associés de Géologie, Pétrologie et Géochimie, Université de Liège, p 161
- Duchesne J-C, Berza T, Liégeois JP, Vander Auwera J (1998) Shoshonitic liquid line of descent from diorite to granite: the late Precambrian post-collisional Tismana pluton (South Carpathians, Romania). *Lithos* 45:281–303. doi:10.1016/S0024-4937(98)00036-X
- Féménias O (2003) Contribution à l'étude du magmatisme tardi- à post-orogénique. De sa source à sa mise en place en sub-surface : exemples régionaux de l'essai de filons du Motru (Roumanie) et du complexe lité profond sous Beaunit (France), PhD dissertation, Université Libre de Bruxelles. p 450
- Féménias O, Coussaert N, Bingen B, Whitehouse M, Mercier J-CC, Demaiffe D (2003) A Permian underplating event in late- to post-orogenic tectonic setting. Evidence from the mafic-ultramafic layered xenoliths from Beaunit (French Massif Central). *Chem Geol* 199:293–315. doi:10.1016/S0009-2541(03)00124-4
- Féménias O, Diot H, Berza T, Gauffriau A, Demaiffe D (2004) Asymmetrical to symmetrical magnetic fabric of dikes: paleo-flow orientations and paleo-stresses recorded on feeder-bodies from the Motru Dike Swarm (Romania). *J Struct Geol* 26:1401–1418. doi:10.1016/j.jsg.2003.12.003
- Féménias O, Mercier J-CC, Nkono C, Diot H, Berza T, Tatu M, Demaiffe D (2006) Calcic amphibole growth and compositions in calc-alkaline magmas: Evidence from the Motru Dyke Swarm (Southern Carpathians, Romania). *Am Min* 91:73–81. doi:10.2138/am.2006.1869
- Gill JB (1981) Orogenic andesites and plate tectonics. Springer, Heidelberg, p 390
- Grove TL, Elkins-Tanton LT, Parman SW, Chatterjee N, Müntener O, Gaetani GA (2003) Fractional crystallization and mantle-melting controls on calc-alkaline differentiation trends. *Contrib Mineral Petrol* 145:515–533
- Hanson GN (1980) Rare earth elements in petrogenesis studies of igneous systems. *Ann Rev Earth Planet Sci* 8:371–406
- Irvine TN, Baragar WRA (1971) A guide to the chemical classification of the common volcanic rocks. *Can J Earth Sci* 8:523–548
- Kay SM, Mpodozis C, Ramos VA, Munizaga F (1991) Magma source variations for mid-late Tertiary magmatic rocks associated with a shallowing subduction zone and a thickening crust in the central Andes (28 to 35°S). In: Harmon RS, Rapela CW (eds) *Andean Magmatism and its Tectonic Setting*. Geol Soc Am Spec Pap 265:113–137
- Kräutner HG, Năstăseanu S, Berza T, Stănoiu I, Iancu V (1981) Metamorphosed Paleozoic in the South Carpathians and its relation with the pre-Palaeozoic basement, Guide to excursion A, Carpath Balkan Assoc Congr XII, Bucuresti, p 116
- Kräutner H, Berza T, Dimitrescu R (1988) South Carpathians. In: Zoubek V (ed) *Precambrian in younger fold belts*. Wiley, London, pp 633–664
- Kuno H (1968) Differentiation of basalt magmas. In: Hess HH, Poldervaart A (Eds) *Basalts: the Poldervaart Treatise on rocks of basaltic composition*, 2, Interscience, New York, pp 623–688
- Le Bas MJ, Le Maître RW, Streckeisen A, Zanettin B (1986) A chemical classification of volcanic rocks based on the total alkali-silica diagram. *J Petrol* 27:745–750
- Le Maitre RW (ed) (2002) *Igneous rocks. A classification and glossary of terms*, 2nd edn. IUGS-Cambridge University Press, p 236
- Liégeois JP, Berza T, Tatu M, Duchesne JC (1996) The neoproterozoic Pan-African basement from the Alpine Lower Danubian nappe system (South Carpathians, Romania). *Precambrian Res* 80:281–301. doi:10.1016/S0301-9268(96)00019-8
- Manolescu G (1937) Etude géologique et pétrographique dans les Muntii Vulcan (Carpatés Méridionales, Roumanie). *An Inst Geol Rom XVIII*:79–172
- Mattauer M (2004) Orthogneisses in the deepest levels of the Variscan belt are not a Precambrian basement but Ordovician granites: tectonic consequences. *CR. Geosciences* 336(6):487–489. doi:10.1016/j.crte.2004.03.001
- McDonough WF, Sun S-S (1995) The composition of the Earth. *Chem Geol* 120:223–253. doi:10.1016/0009-2541(94)00140-4
- Miller C, Schuster R, Klötzli U, Frank W, Purtscheller F (1999) Post-Collisional Potassic and Ultrapotassic Magmatism in SW Tibet: Geochemical and Sr-Nd-Pb-O Isotopic Constraints for Mantle Source Characteristics and Petrogenesis. *J Petrol* 40:1399–1424
- Miyashiro A (1974) Volcanic rock series in island arcs and active continental margins. *Am J Sci* 274:321–355
- Moghazi AM (2003) Geochemistry and petrogenesis of a high-K calc-alkaline Dokhan Volcanic suite, South Safaga area, Egypt: the role of the late Neoproterozoic crustal extension. *Precambrian Res* 125:161–178. doi:10.1016/S0301-9268(03)00110-4
- Mohamed FH, Moghazi AM, Hassanen MA (2000) Geochemistry, petrogenesis and tectonic setting of late Neoproterozoic Dokhan-type volcanic rocks in the Fatira area, eastern Egypt. *Int J Earth Sci* 88:764–777
- Nkono C, Féménias O, Diot H, Berza T, Demaiffe D (2006) Flowage differentiation in an andesitic dyke of the Motru swarm (S. Carpatian, Romania): evidence from AMS, CSD and geochemical investigations. *J Volcan Geotherm Res* 154:201–221. doi:10.1016/j.jvolgeores.2006.02.011
- Nomade S, Renne PR, Mo X, Zhao Z, Zhou S (2004) Miocene volcanism in the Lhasa block, Tibet: spatial trends and geodynamic implications. *Earth Planet Sci Lett* 221(1–4):227–243. doi:10.1016/S0012-821X(04)00072-X
- Pavelescu L (1953) Studiul geologic și petrographic al regiunii centrale și de Sud-Est a Muntilor Retezatului. *An Com Geol XXV*:119
- Pearce JA (1982) Trace element characteristics of lavas from destructive plate boundaries. In: Thorpe RS (ed) *Andesites*. Wiley, Chichester, pp 525–548
- Pearce JA, Peate DW (1995) Tectonic implications of the composition of volcanic arc magmas. *Ann Rev Earth Planet Sci* 23:251–285
- Pearce JA, Harris NBW, Tindle AG (1984) Trace element discrimination diagrams for the tectonic interpretation of granitic rocks. *J Petrol* 25:956–983

- Peccerillo A (1985) Roman comagmatic province (central Italy): evidence for subduction-related magma genesis. *Geology* 13:103–106
- von Raumer JF, Stampfli GM, Bussy F (2003) Gondwana-derived microcontinents – the constituents of the Variscan and Alpine collisional orogens. *Tectonophysics* 365(1–4):7–22. doi:10.1016/S0040-1951(03)00015-5
- Richards JP, Villeneuve M (2002) Characteristics of late Cenozoic volcanism along the Archibarca lineament from Cerro Lullailaco to Corrida de Cori, northwest Argentina. *J Volcanol Geotherm Res* 116:161–200. doi:10.1016/S0377-0273(01)00329-8
- Rickwood PC (1989) Boundary lines within petrologic diagrams which use oxides of major and minor elements. *Lithos* 22:247–263. doi:10.1016/0024-4937(89)90028-5
- Rock NMS (1984) Nature and origin of calc-alkaline lamprophyres: minettes, vogesites, kersantites, and spessartites. *Trans R Soc Edinburgh* 74:193–227
- Rogers NW, Hawkesworth CJ, Parker RJ, Marsh JS (1985) The geochemistry of potassic lavas from Vulsini, central Italy, and implications for mantle enrichment processes beneath the Roman region. *Contrib Mineral Petrol* 90:211–257
- Rogers NW, Hawkesworth CJ, Matthey DP, Harmon RS (1987) Sediment subduction and the source of potassium in orogenic leucitites. *Geology* 15:451–453
- Rottura A, Bargossi GM, Caggianelli A, Del Moro A, Visona D, Tranne CA (1998) Origin and significance of the Permian high-K calc-alkaline magmatism in the central-eastern Southern Alps, Italy. *Lithos* 45:329–348. doi:10.1016/S0024-4937(98)00038-3
- Rutherford MJ, Devine JD (1988) The May 18, 1980 eruption of Mont St. Helens 3. Stability and chemistry of amphibole in magma chamber. *J Geophys Res* 93:11949–11959
- Savu H (1970) Structura plutonului granitoid de Șușița și relațiile sale cu formațiunile autohtonului danubian (Carpații Meridionali). *D S Inst Geol LVI/5*:123–153
- Sisson TW (1994) Hornblende-melt trace-element partitioning measured by ion microprobe. *Chem Geol* 117:331–344. doi:10.1016/0009-2541(94)90135-X
- Sloman LE (1989) Triassic shoshonites from the Dolomites, northern Italy, alkaline arc rocks in a strike-slip setting. *J Geophys Res* 94:4655–4666
- Snetsinger KG (1969) Manganoan ilmenite from a sierran adamellite. *Am Min* 54:431–436
- Stănoiu I (1973) Zona Mehedinți – Retezat: o unitate paleogeografică și tectonică distinctă a Carpaților Meridionali. *D S Inst Geol LIX/5*:127
- Stampfli GM, Borel GD (2002) A plate tectonic model for the Paleozoic and Mesozoic constrained by dynamic plate boundaries and restored synthetic oceanic isochrons. *Earth Planet Sci Lett* 196(1–2):17–33. doi:10.1016/S0012-821X(01)00588-X
- Thirwall MF (1988) Wenlock to mid-Devonian volcanism of the Caledonian-Appalachian Orogen. *Geol Soc Lond Spec Publ* 38:415–428
- Turner SP, Platt JP, George RMM, Kelly SP, Pearson DG, Norwell GM (1999) Magmatism associated with orogenic collapse of the Betic-Alboran Domain, S.E. Spain. *J Petrol* 40:1011–1036
- Vander Auwera J, Bologne G, Roelands I, Duchesne J-C (1998) Inductively coupled plasma-mass spectrometric (ICP-MS) analysis of silicate rocks and minerals. *Geol Belg* 1:49–53
- Wang K-L, Chung S-L, Chen C-H, Shinjo R, Yang TF, Chen C-H (1999) Post-collisional magmatism around northern Taiwan and its relation with opening of the Okinawa Trough. *Tectonophysics* 308:363–376. doi:10.1016/S0040-1951(99)00111-0
- Wilson M (1989) *Igneous Petrogenesis*. Unwin Hyman, London, p 457
- Winter JD (2001) *An introduction to Igneous and Metamorphic Petrology*. Prentice-Hall, Upper Saddle River, p 697
- Wones DR, Eugster HP (1965) Stability of biotite: experiment, theory and application. *Am Min* 50:1228–1272
- Zellmer G, Hawkesworth CJ, Sparks RSJ, Thomas LE, Harford CL, Brewer TS, Loughlin SC (2003) Geochemical evolution of the Soufriere Hills Volcano, Montserrat, Lesser Antilles Volcanic Arc. *J Petrol* 44:1349–1374
- Zhou J (1985) The timing of calc-alkaline magmatism in parts of the Alpine-Himalayan collision zone and its relevance to the interpretation of Caledonian magmatism. *J Geol Soc* 142:309–317